Superconductor Science and Technology

PAPER

Large enhancement of the in-field critical current density of YBCO coated conductors due to composite pinning landscape

IOP Publishing Superconductor Science and Technology
Supercond. Sci. Technol. **34** (2021) 015011 (13pp) https://doi.org/10.1088/1361-6668/ab9f64

Large enhancement of the in-field critical current density of YBCO coated conductors due to composite pinning landscape

K J Kihlstrom[1,7], L Civale[2], S Eley[2,8], D J Miller[1], U Welp[1], W K Kwok[1], P Niraula[3], A Kayani[3], G Ghigo[4,5], F Laviano[4,5], S Fleshler[6], M Rupich[6] and M Leroux[1,2,9]

[1] Materials Science Division, Argonne National Laboratory, Argonne, IL 60439, United States of America
[2] Condensed Matter and Magnet Science, Los Alamos National Laboratory, Los Alamos, NM 87545, United States of America
[3] Department of Physics, Western Michigan University, Kalamazoo, MI 49008, United States of America
[4] Department of Applied Science and Technology, Politecnico di Torino, 10129, Torino, Italy
[5] Istituto Nazionale di Fisica Nucleare, Sez. Torino, 10125, Torino, Italy
[6] American Superconductor Corp., 114 East Main Street, Ayer, MA 01432, United States of America
[7] Physics Department, City University of New York, Queens College, 65-30 Kissena Blvd, Flushing, NY 11367, United States of America
[8] Present address: Department of Physics, Colorado School of Mines, Golden, CO 80401, United States of America

E-mail: welp@anl.gov

Received 25 February 2020, revised 20 April 2020
Accepted for publication 23 June 2020
Published 30 November 2020

Abstract

$YBa_2Cu_3O_7$-based coated conductors (CCs) achieve the highest critical current densities (J_c) of any known superconductor and are a key technology for applications such as rotatory machines, high-field magnets and power transmission. Incorporation of nano-sized non-superconducting second phases as additional vortex pinning centers has been considered the most amenable route to further enhance J_c at an industrial scale, and has been successfully used in commercial CCs. The resulting pinning landscape is quite complex, with both synergistic and competing interactions among the various types of defects. Particle irradiation, on the other hand, allows for a controlled post-processing incorporation of a well-defined defect morphology. We have previously shown that irradiation with protons and other light ions can further enhance the in-field J_c in commercial state-of-the-art CCs. Here we develop a combined irradiation process that increases J_c above values previously achieved by irradiating with only one species. Our new approach involves sequentially irradiating with 250 MeV Au ions and 4 MeV protons. For example, at $T \sim 27$ K (liquid neon) and $\mu_0 H \sim 4$ T, a region of interest for rotatory machines applications, we obtain $J_c \sim 5$ MA cm^{-2}, which is about 40% higher than the values produced

[9] Present address: Laboratoire National des Champs Magnétiques Intenses (CNRS, EMFL, INSA, UGA, UPS), Toulouse 31400, France

by the individual irradiations. Finally, we conclude that this is due to the synergistic pinning effects of the introduced splayed, non-uniform columnar defects and small clusters.

Keywords: coated conductor, superconductors, critical current, vortex pinning, composite pinning landscape

(Some figures may appear in colour only in the online journal)

1. Introduction

Coated conductors (CCs), $YBa_2Cu_3O_7$ (YBCO) films deposited on flexible metal tapes, are a leading technology for superconductor applications. CCs can be produced in lengths exceeding 1 km, and are currently being used in prototypes of power transmission lines, motors, generators, fault current limiters and high-field or Tokamak magnets [1–6]. Sustained research has led to tremendous improvement in the performance of CCs, enhancing the critical current density (J_c) by orders of magnitude over pristine YBCO single crystals [7–26]. In fact, at low temperatures (T) and magnetic fields (H), YBCO films and CCs have the strongest vortex pinning of any known superconductor, with J_c values above 50 MA cm^{-2} (e.g. see Gutierrez *et al* [12] and [15]), exceeding those in any other superconducting wires (such as NbTi) by at least an order of magnitude [27]. Thus, besides the obvious technological impact, understanding pinning in this extreme case has general scientific interest. Specifically, the rapid decrease of J_c as H increases has thwarted more widespread deployment of CCs, therefore further understanding of vortex matter and improvements in J_c at high fields are critical.

The strong pinning in CCs is a consequence of their mixed pinning landscapes, which are the most effective due to at least two reasons: First, due to changes in the vortex size and density with T and H, different types of disorder will be most effective at pinning vortices in different regions of the H-T phase diagram [7]. Second, some combinations of disorder produce beneficial synergistic effects [15, 28], such as reducing creep rates. However, the interactions among different types of disorder (such as randomly distributed nanoparticles and point defects, columnar defects, twin boundaries and stacking faults) can also produce detrimental competitive effects [28, 29].

To further improve the performance of CCs beyond the J_c values achieved by the already quite effective as-grown pinning landscape of 'standard' YBCO films [7], additional disorder must be introduced. There are two common ways to do this: chemical incorporation of non-superconducting second phases [7–26] and irradiation damage [30]. The former is now standard in commercial CCs because it has proven industrially-scalable. However, the chemically added defects (e.g. nanoparticles or nanorods) not only interact with, but also alter pre-existing pinning centers, such as twin boundaries and stacking faults, in ways that are difficult to anticipate and control.

Particle irradiation, on the other hand, allows controlled introduction of well-defined types and densities of disorder, thus providing a valuable tool to engineer pinning landscapes and improve our understanding of vortex matter. The nature of the damage produced under different irradiation conditions in YBCO is well known and understood [31–38]. Numerous studies have been performed on clean single crystals, where the low pre-irradiation J_c can be enhanced by orders of magnitude and the interpretation of the resulting J_c is relatively straightforward [39–47]. However, the use of particle irradiation to improve vortex pinning in coated conductors is relatively unexplored [48–54]. Combining different types of irradiations enables the controlled design of mixed pinning landscapes, but even fewer studies have been published [55, 56].

Clearly, since coated conductors display already high J_c, corresponding to a significant fraction of the absolute limit set by the depairing current density, the dramatic increases observed in single crystals are not expected here. Nevertheless, a doubling of J_c at high fields ($\sim$6 T) and intermediate temperatures ($\sim$27 K), using post-fabrication proton irradiation, has been obtained in commercial CCs [48]. Even more remarkable was the subsequent demonstration that essentially the same beneficial effects could be obtained by oxygen irradiation using a dose 3 orders of magnitude smaller [49]. This allowed the irradiation to be done at a rapid rate of just one second per cm^2, compatible with the tape speed on a CC production line, thus enabling the use of this tool at industrial scale. Indeed, broad J_c improvements using reel-to-reel 16 MeV Au^{5+} irradiation of 46 mm wide production tapes were subsequently achieved [50].

Here, we further build on those previous studies [48–51] by exploring the pinning effects of compound defects, introduced in production line CCs by irradiation with 250 MeV gold ions and 4 MeV protons. We achieve J_c values that surpass those previously reached with proton irradiation and extend over a much wider field range ($J_c \sim 13$ MA cm^{-2} and 6 MA cm^{-2} at 27 K in applied fields of 1 T||c and 6 T||c, respectively). We use the T and H dependencies of J_c and the vortex creep rates (S) to investigate the contribution of the two types of disorder and the synergy between them.

2. Experimental details

The samples studied here are Dy-doped YBCO films manufactured by American Superconductor Corp (AMSC), with nominal thickness $\delta = 1.2$ μm (based on a YBCO coating of 7200 mg m^{-2} and excluding porosity and added Dy_2O_3), deposited by MOD (metal organic deposition) onto RABiTS™ substrates (Rolling Assisted Bi-axially Textured Substrates) [16, 48–51, 57–59]. All samples are capped with a 0.8 um thick Ag-layer protecting the superconducting film.

The samples were irradiated with 250 MeV gold ions (Au^{+17}) along the c-axis at room temperature to a dose-equivalent matching field $B_\chi = 3$ T, using the Tandem-XTU facility of the LNL laboratories of the Italian National Institute for Nuclear Physics (INFN). The ion beam was normal to the YBCO CCs (parallel to the c-axis), and the ion flux was kept below 1.8×10^8 cm^{-2} s^{-1} to avoid sample damage due to heating. After characterization, these samples were irradiated with 4 MeV protons along the c-axis at the 6 MeV tandem van de Graaff accelerator at Western Michigan University [48, 49]. A gold foil was used to homogenize the beam over an area of ∼1 cm diameter, and typical p-beam currents of 0.5 μA were used, in addition to a cooling stage to prevent sample heating. All irradiations occurred through the protective Ag-layer.

Magnetization (**M**) studies were performed in two commercial Quantum Design SQUID magnetometers using 3×5 mm^2 rectangular samples, patterned by photolithography and Ar-ion milling. One of the magnetometers was used to measure $M(H)$ loops at various T for **H**||c-axis, i.e. normal to the film surface, and $J_c(H, T)$ was determined from the width of the hysteresis, ΔM, using the Bean critical state model [60]. The second magnetometer was used to investigate the flux creep as a function of T and H, for **H**||c-axis. To prepare an initial fully penetrated critical state for the creep studies, first a large enough negative field was applied, then the field was swapped to the measuring field $H > 0$ and a few data points (typically 8) were measured in this *field increasing* or *lower* branch [51]. Subsequently the field was increased to a high enough positive value and finally decreased again to the measuring H, where the time decay of **M** on this *field decreasing* or *upper* branch was recorded over a period of ∼1 h. The initial points on both branches were averaged to obtain $\mathbf{M}_{avg}$, which was subtracted from **M** to obtain the irreversible contribution $\mathbf{M}_{irr}$ associated with the critical state, and the creep rates were calculated as $S_{l,t} = -\,\mathrm{d}(\ln M_{irr,l,t})/\mathrm{d}(\ln t)$. Transport measurements at 27 K were performed using conventional four-terminal geometry on 0.065 mm × 4.0 mm bridges patterned by photolithography and Ar ion milling.

Characterization of the defect structure was carried out using high-resolution and diffraction contrast transmission electron microscopy (TEM) [48, 49]. TEM samples were prepared by focused ion beam (FIB) lift-out methods followed by low-energy Ar ion milling. This approach minimizes artifacts due to specimen preparation. Several TEM samples were prepared from different regions of each sample to ensure that results were representative of each condition. The pinning landscape of pristine MOD-CCs, such as those used in this study, is already very complex. As shown in the TEM image in figure 1(a), it contains randomly distributed Dy_2O_3 nanoparticles (NPs) that are ∼30 nm in diameter, which are purposely introduced during fabrication, in addition to a small density of larger $Y_2Cu_2O_5$ NPs, twin boundaries and stacking faults, all of which appear spontaneously during synthesis [16, 51, 57–59]. There are also point defects, not visible in the TEM images.

3. Results and discussion

3.1. Microstructure

Proton irradiation has been extensively used to enhance the vortex pinning in superconductors [39, 40]. Earlier TEM work on YBCO showed that p^+ irradiation produces a hierarchy of randomly distributed defects with sizes ranging from atomic scale (Frenkel pairs), mostly on the O and Cu sites, to clusters that are 2–5 nm in diameter [35, 48, 51]. A typical TEM image for a p^+-irradiated sample [48] similar to the pieces used in this study is shown in figure 1(b). Ultimately, the reason for the effectiveness of p^+ or other light-ion irradiations (such as O) is that pinning in the pristine AMSC CC is dominated by the Dy_2O_3 NPs, which are particularly effective at low fields where the intervortex distance is of the order of, or larger than, the average distance among NPs. At higher H there are not enough NPs and their effectiveness decreases. At near-optimum p^+ doses the densities of the smaller irradiation-induced defects are orders of magnitude higher than that of the NPs, allowing the irradiation induced defects to remain effective pinning centers at high H.

3.2. Critical current

Figure 2 shows the dose dependence of J_c in our proton-irradiated CC sample. Due to the competition between increasing pinning force and decreasing superconducting volume fraction, a non-monotonic dependence of J_c on irradiation dose, i.e. pinning sites concentration, is theoretically expected [61, 62]. This behavior is observed in figure 2. We found that, although J_c reaches its maximum at a dose that is temperature and field dependent, a dose of $\sim 18 \times 10^{16}$ p^+ cm^{-2} is a good compromise over a broad T and H range that is technologically relevant. Note that this relatively high dose of irradiation only induces a modest reduction of T_c. As shown in figure 3(a), the suppression rate of T_c is only 0.2 K per 10^{16} p^+ cm^{-2}, which is much less than in single crystals. Also, no broadening appears in the magnetization curves around T_c (figure 3(b)) evidencing the homogeneity of the irradiations. A possible reason for this small suppression rate of T_c in coated conductors is that the numerous big defects and nanoparticles, which are already present in the pristine sample, act as sinks for the mobile point defects induced during irradiation. Isolated point defects are indeed the type of defects with the strongest impact on T_c (pair-breaking from electronic scattering in a d-wave), whereas the large columnar defects and clusters are much bigger and thus are weaker scattering centers, i.e. less 'pair-breaking' [63].

Figure 4 shows J_c vs. H at four temperatures, as obtained from magnetization measurements for a pristine piece of CC (black squares) that was subsequently irradiated with Au (red circles) then protons (blue diamonds), as well as a piece from the same batch that was irradiated to 18×10^{16} p^+ cm^{-2} (green triangles). This last piece is the one that was studied after repeated irradiation in figure 2. We first note that at $T = 5$ K (figures 4(a)) and $(H) \sim 0$, the J_c of this CC is higher

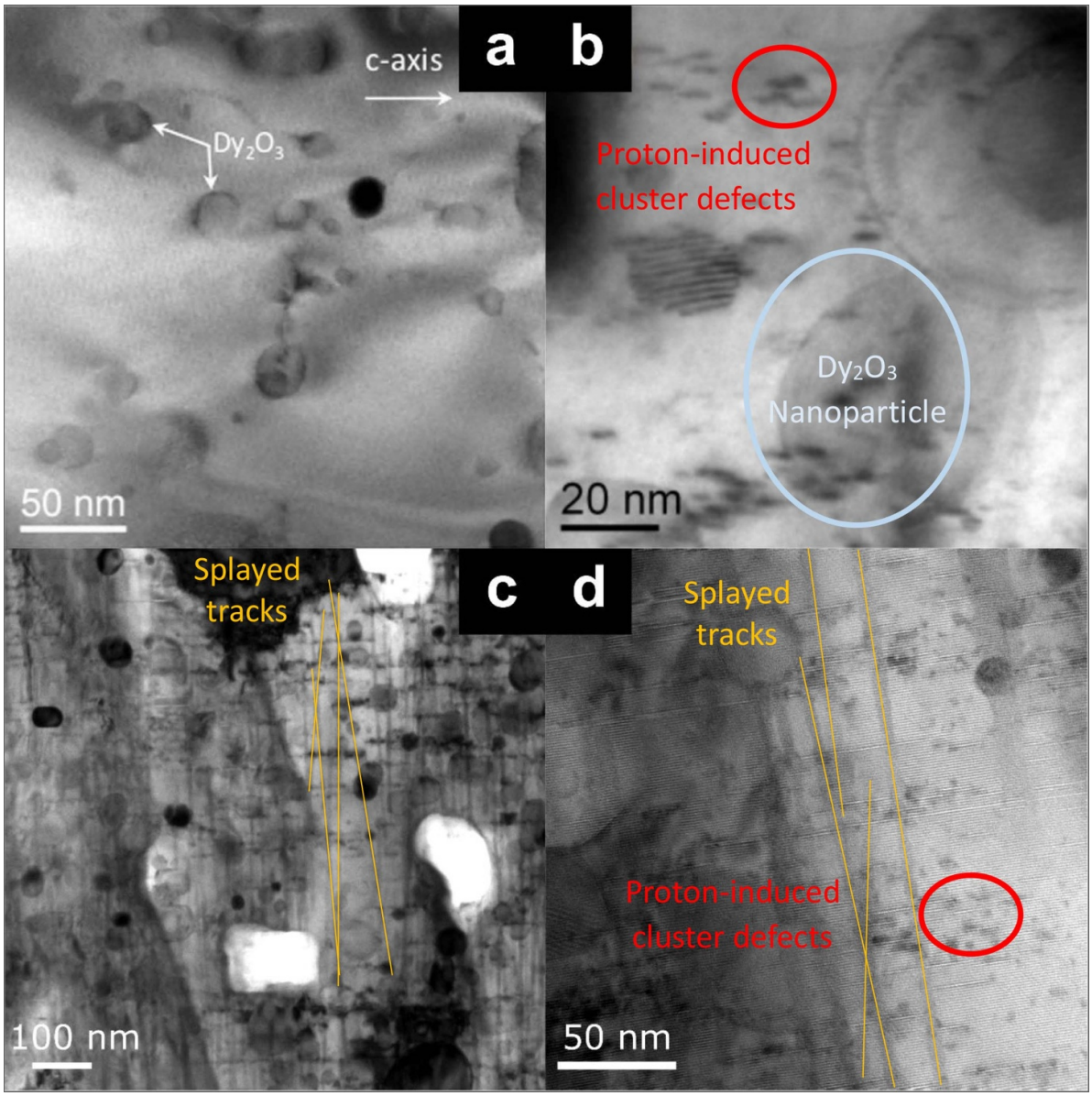

Figure 1. Bright field TEM images representative of the samples studied in this paper: (a) a pristine as-grown MOD-CC with Dy_2O_3 nanoparticles; (b) a proton irradiated MOD-CC, with ∼5 nm sized irradiation-induced clusters. (c)–(d) a CC piece with compound defects: splayed, non-uniform tracks ∼7 nm in diameter created by Au irradiation and small defect clusters created by proton irradiation. Image (a) reproduced from Eley *et al* [51]. Image (b) reproduced from Jia *et al* [48]. Appl. Phys. Lett. **103** 122 601 (2013) (https://doi.org/10.1063/1.4821440), with permission of AIP Publishing.

than the J_c reported for YBCO single crystals irradiated at any conditions. We also observe the typical fast decay in $J_c(H, T)$ as H or T are increased.

In figures 5(a–d) we plot the field dependence of the J_c enhancement factors, $J_c(H,T)/J_c^{pristine}(H,T)$ for the same temperatures as in figure 4 so as to facilitate the comparison of the effectiveness of proton, gold and gold + proton irradiations. Firstly, let us consider the optimum 4 MeV p^+ irradiation: from figures 4(a–c) and 5(a–c), we see that for $T \leq 50$ K the effect goes from detrimental to beneficial (i.e. J_c increases as compared to the pristine sample) above a crossover field H_{cr}, with $\mu_0 H_{cr} \sim 0.6$ T at 5 K (figures 4(a) and 5(a)), increasing to ∼1 T at 50 K (figures 4(c) and 5(c)). For $T = 77$ K, the effect of the (optimum) p^+ irradiation is detrimental at all fields (figures 4(d) and 5(d)). This suppression of J_c at low H following p^+ irradiation is likely caused by competing (as opposed to synergistic) pinning effects. Creep studies show that such competition arises at least in part from faster creep due to lower activation energies following irradiations [51].

Now, let us consider the case of Au irradiation. Columnar defects (CDs) produced by swift heavy-ion irradiation are the most effective pinning centers for H||CDs and below the matching field (B_Φ), because the whole length of the cores of all the vortices can be trapped [45]. They also retain their effectiveness up to higher T than point defects, due to their larger pinning energy. For both reasons, they are natural candidates to complement the effect of the p^+ irradiations.

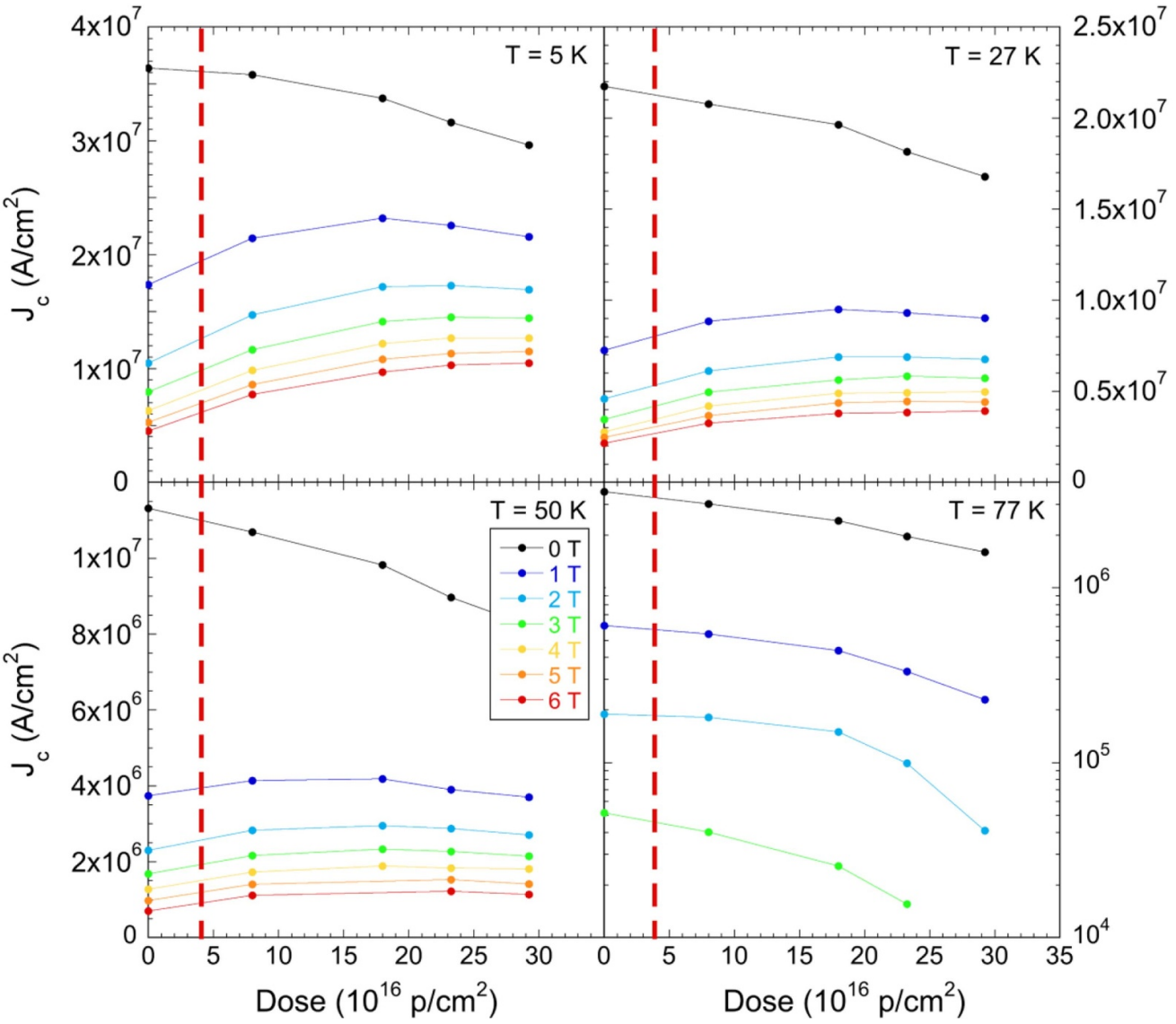

Figure 2. Critical current density (J_c) vs. dose, for the sample irradiated with 4 MeV protons, at several applied magnetic fields (H) and for $T = 5$, 27, 50 and 77 K. The vertical dotted lines indicate the proton dose used in the combined-irradiations (4×10^{16} p cm^{-2}).

As a first step in our combined irradiation landscape engineering, we irradiated our sample with 250 MeV Au ions. We selected this relatively low energy heavy-ions to create CDs that are *splayed* and *inhomogeneous* along their length, because these features are known to produce the beneficial effect of slowing down the vortex dynamics due to low-energy kink excitations [15, 64, 65], as will be described below. The presence of CDs with these characteristics is clearly observed in figures 1(c and (d)), which were obtained on the piece of CC used in this study after all irradiations and measurements were completed. The diameter of the CDs is ∼7–8 nm, somewhat larger than the diameter of the vortex cores, $2\sqrt{2}\xi_{ab}(T)$, which is ∼5 nm for YBCO at $T \ll T_c$, making them effective pins (here ξ_{ab} is the in-plane coherence length). We chose a dose-equivalent matching field $B_\phi = 3$ T which is somewhat lower than the optimum B_ϕ for J_c enhancement reported in the literature for YBCO [66], and is also in the range of target magnetic fields for rotating machinery applications [1].

The red symbols in figures 4 and 5 show J_c and $J_c/J_c^{pristine}$ respectively, after the 250 MeV Au ions irradiation. The dissimilar effects of the p^+ and Au irradiations are apparent. First, for $T \leq 27$ K the Au irradiation produces no detrimental effect at low H; in fact, there is even a small increase in $J_c(H = 0, T = 5$ K) (figures 4(a, b) and 5(a, b)). For $T = 50$ K a slight deterioration occurs at low field, but it is less pronounced than for p^+ and H_{cr} is much smaller (figures 4(c) and 5(c)). For $T \leq 50$ K the enhancement factor for the Au irradiation first increases with H, similarly to the p^+ irradiation, but then maximizes at an intermediate field ∼1.5 T–2 T and, in contrast to the p^+ case, decreases for higher fields as most CDs become occupied and vortices in between the CDs start to proliferate. At $T = 5$ K, the 250 MeV Au processing becomes less

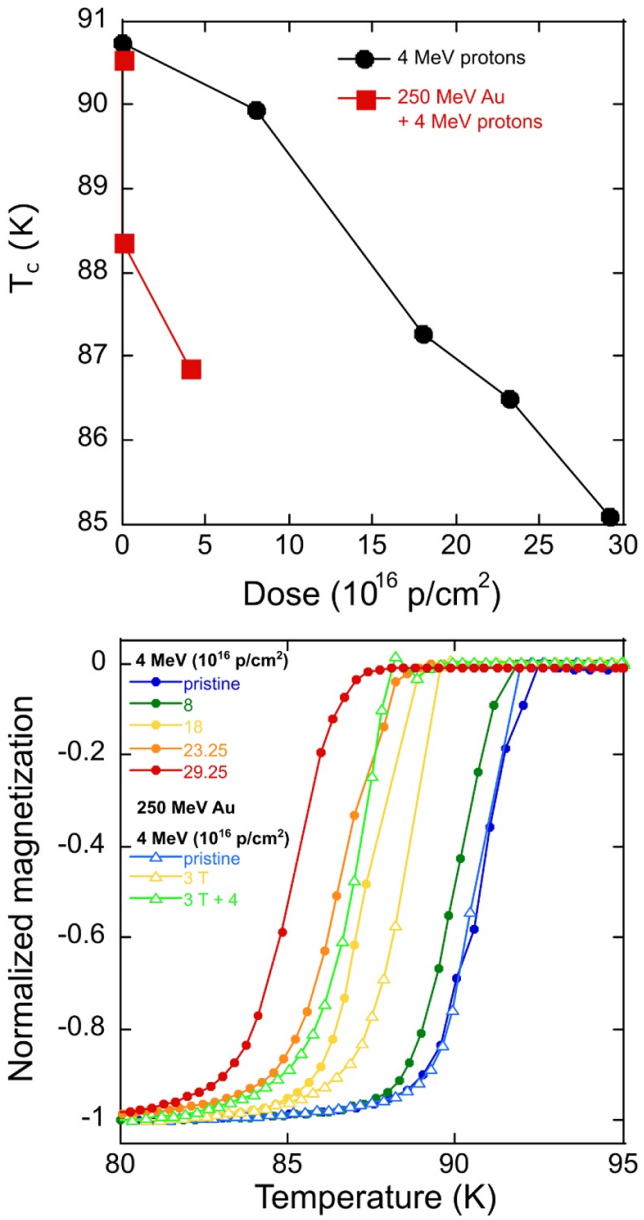

Figure 3. (a) Critical temperature as a function of proton irradiation dose for both the proton-irradiated sample and the combined Au + proton-irradiated sample. (b) Magnetization measurements from which T_c was determined. The labels indicate the proton (circles), Au (triangles), and combined doses (green triangle).

effective than the 4 MeV p^+ processing at ~4 T, i.e. just above B_ϕ. However, as T increases the larger pinning energy of the CDs (due to their longer length) comes into play such that at 27 K the CDs remain better up to ~5 T, and at 50 K they remain superior all the way up to our maximum field.

The $T = 77$ K results (figures 4(d) and 5(d)) deserve particular consideration. First, the low H deterioration is as bad for Au as for p^+ irradiation, with $J_c(H \sim 0, T = 77K)/J_c^{pristine}(H \sim 0, T = 77K) \sim 0.5$, and T_c suppression is also similar in both cases: 88.4 K and 87.3 K respectively, see figure 3. However, at high H the Au irradiation does improve J_c, in sharp contrast to the p^+ case. It must be recognized that the dramatic enhancement factors (>10) at high H are a consequence of the very small J_c of the pristine sample. Nevertheless, a critical current density $J_c(H = 4\ \text{T}, T = 77\ \text{K}) \sim 0.1$ MA cm^{-2} is encouraging and would enable applications of CC refrigerated by liquid N_2.

The fact that the Au irradiation has almost no effect at $H \sim 0$ and low T is not trivial and clearly evidences that pinning is not additive. At low fields, a material may have enough strong pinning centers to pin all the vortices very effectively. In a simple scenario, adding weaker defects will not create better pinning configurations; vortices will just 'ignore' them and J_c will be unaltered. The rich landscape of the pristine CC contains a small density of pinning centers (or combinations of them) that are very strong. As H increases those few defects become saturated and the much larger density of CDs progressively increase their fractional contribution to J_c, as we observed. We know, however, that this cannot be the complete picture, as, in contrast to Au irradiation, p^+ irradiation decreases J_c at $H \sim 0$ as already discussed.

After examining the effect of proton and Au irradiation independently, we combined both: the piece irradiated with Au was also irradiated with 4 MeV p^+. We selected a dose of 4×10^{16} p^+ cm^{-2}, well below the optimum for p^+ irradiation alone to avoid excessive damage, but large enough to produce significant J_c enhancement in a pristine CC, as shown by the right dashed line in figure 2. The small defect clusters created by this second irradiation are visible in figure 1(d). Note that it is well-known that p^+ irradiation also creates point defects, but these are not visible in these TEM images. The resulting $J_c(H, T)$ and $J_c(H,T)/J_c^{pristine}(H,T)$ curves are shown as blue diamonds in figures 4 and 5, respectively. It is apparent that the mixed landscape created by this *combined irradiation* produces better performance than either the 250 MeV Au or the 4 MeV p^+ alone. The yellow colored areas in figure 5 highlight the additional synergistic J_c enhancement produced by the combined irradiations, as compared to either of the individual ones. Below ~1 T and for all T, the J_c resulting from the combined irradiation process is marginally smaller than the Au result, but for $\mu_0 H > 1$ T and $T \leq 50$ K it produces clearly stronger pinning. As seen in figure 5(b), for $T = 27$ K and fields in the 4–6 T range, a regime particularly relevant for superconducting rotatory machines, the combined irradiation exceeds the effect of the individual ones by roughly a factor of two. This unforeseen synergetic effect is the central result of this study. In figure 2, one can also see that at 27 K/4 T a proton irradiation dose of 4.10^{16} p cm^{-2} should yield $J_c \sim 3.5$ MA cm^{-2} and from figure 4(b) one can see that the $B_\chi = 3$ T Au irradiation also yields $J_c \sim 3.8$ MA cm^{-2} at 27 K/4 T. Hence, the value $J_c \sim 5.1$ MA cm^{-2} of the combined irradiations ($B_\chi = 3$ T Au + 4.10^{16} p cm^{-2}) is about 40% higher than either individual irradiations. We believe this synergy stems from the concept of a mixed pinning landscape [28, 48], in which the randomly distributed localized defects from proton irradiation catch stray vortices and suppress vortices jumping between CDs (for instance by hampering double kinks expansion, cf part 3.3). For $T = 77$ K, the combined irradiation just replicates the Au irradiation result, which confirms

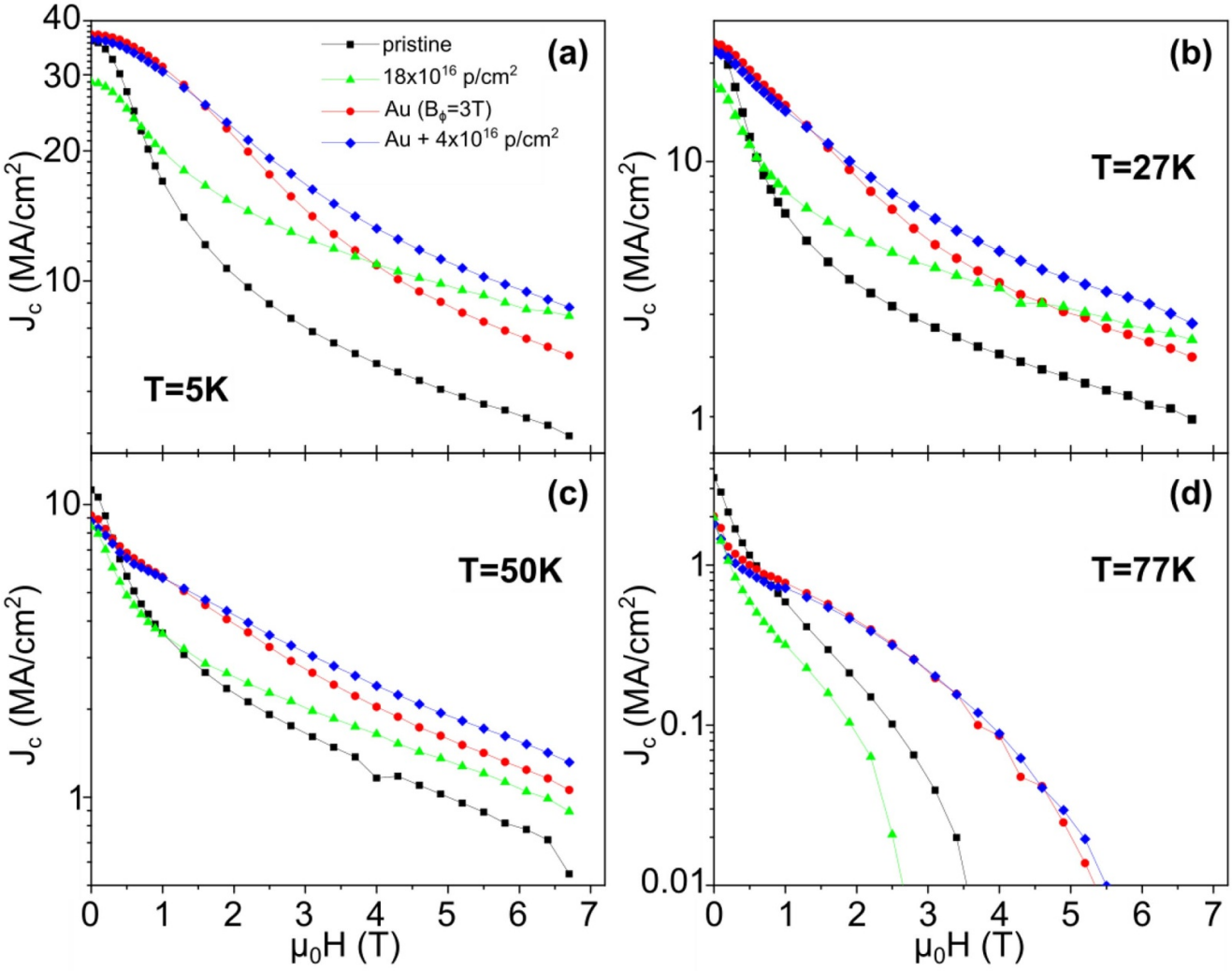

Figure 4. Critical current density (J_c) measured by magnetization vs. applied magnetic field (H) at four temperatures, in samples from the same batch, for: (black squares) a pristine CC; (green triangles) a CC irradiated to the optimum proton dose (see text); (red circles) a CC piece irradiated with Au; and (blue diamonds) the same CC piece after both Au and proton irradiation.

the ineffectiveness of p^+ irradiation induced defects at 77 K, as already observed in figure 2.

In summary, at intermediate magnetic fields and all temperatures in figure 4, the blue curve of combined Au and proton irradiation is above all others thanks to the synergy between defects. Then at high magnetic field and low temperature the best pinning centers are the numerous clusters and Frenkel pairs generated by proton irradiation which can accommodate a large number of vortices [48], whereas the columnar defects from gold irradiation are saturated with vortices above the matching field of 3 T. Hence, in figure 4 the green curve (18×10^{16} p^+ cm^{-2}) shows higher J_c than the red curve (Au, $B_\phi = 3$ T) at high magnetic field and low (a) or intermediate (b) temperature. At high temperature (77 K, figure 4(d)) however, the defects from proton irradiation are too small and weak to pin vortices efficiently whereas the long columnar defects retain their strong pinning properties.

Finally, to confirm that the CDs produced by Au irradiation indeed act as correlated pinning centers in our samples, we performed angular-dependent transport studies of J_c on a bridge patterned from the same CC batch. Figure 6 shows J_c vs. the angle between **H** and the c-axis (Θ), at $T = 27$ K and $\mu_0 H = 6$ T, for that bridge before and after irradiation with 250 MeV Au to a dose equivalent $B_\phi = 3$ T. In the pristine state, $J_c(\Theta)$ shows the typical anisotropy of AMSC CCs, with a large maximum centered at **H**||ab associated with correlated pinning by stacking faults, and a small c-axis peak due to twin boundaries. After irradiation, a much larger c-axis peak demonstrates the correlated pinning of the artificial CDs.

3.3. Vortex creep

Additional information about the pinning landscape can be obtained from the vortex dynamics, in particular from the normalized flux creep rates [67–69] $S(T, H)$. Such information is complementary because of the quite different dependences of J_c and S on disorder. The former is very sensitive to the details of the pinning landscape, and consequently J_c values differing by orders of magnitude, as well as countless variations of the $J_c(T, H, \Theta)$ functional dependences, have been reported for

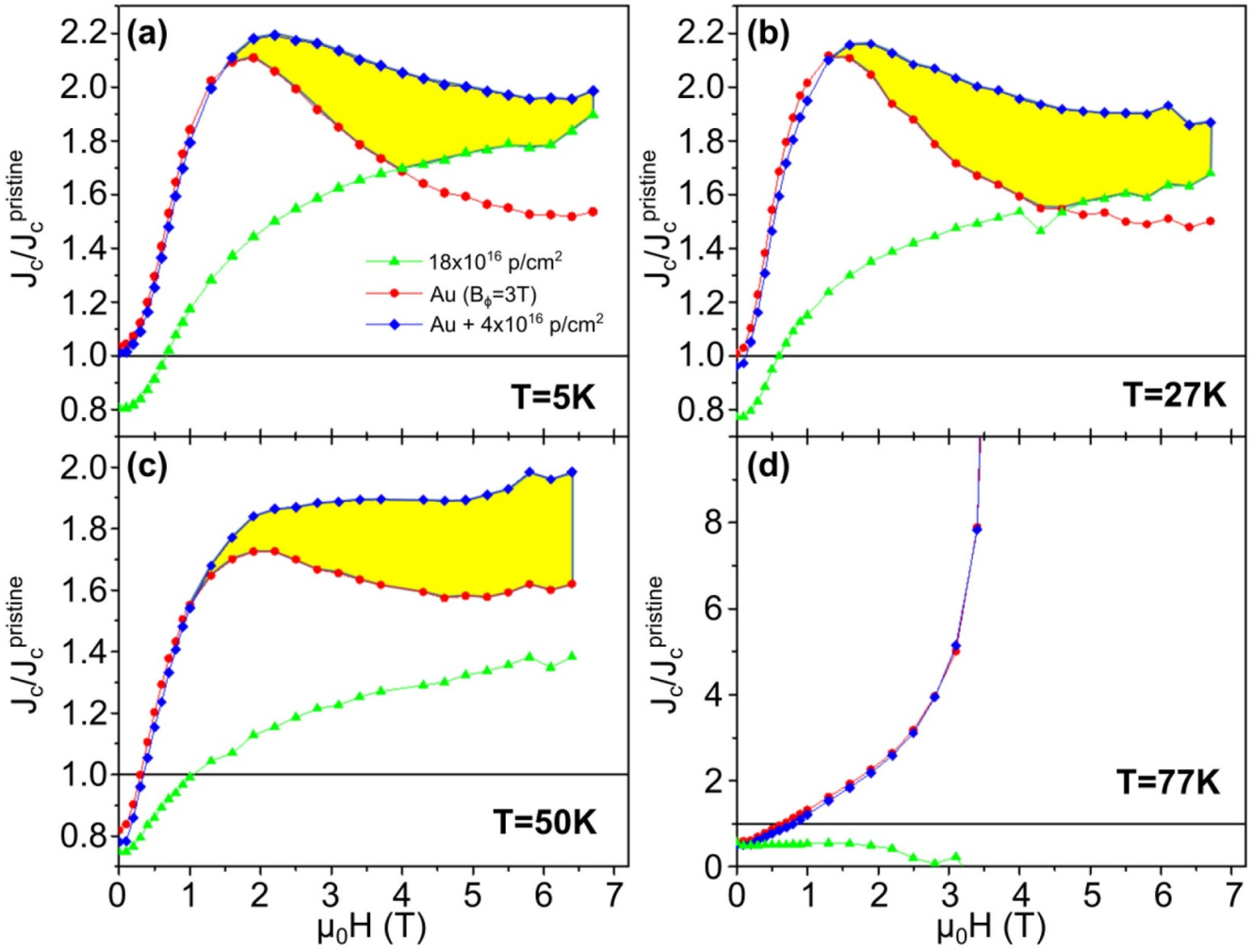

Figure 5. Critical current density enhancement factors, $J_c(H,T)/J_c^{pristine}(H,T)$, for the same samples and at the same temperatures shown in figure 4. The yellow colored areas show the *T*-*H* regions where the combined irradiation produces stronger pinning than any of the individual ones.

YBCO. In contrast, creep rates in YBCO exhibit much less variability, with absolute values that are similar in all cases and functional dependences that typically fall into one of a few categories.

The reason for this is that $S(T, H)$ is mainly defined by the type of the dominant depinning excitations, rather than by the quantitative values of the pinning parameters [68]. First, the dynamics can be either glassy or plastic [70–72]. In the first case the size of the excitation (either a vortex segment or a vortex bundle) diverges in the limit of $J \to 0$, and consequently the flux creep activation energy diverges as $U(J) \propto U_p \times (J_c/J)\mu$, where $U_p(T, H)$ is the pinning energy and $\mu > 0$ is the glassy exponent. In the second case, in contrast, the size and the activation energy of the excitation remain finite for $J \to 0$ and the low J behavior $U(J) \propto U_p \times (J_c/J)^p$ is characterized by a plastic exponent $p < 0$. Within each category, different excitations produce different exponents. For instance, in collective pinning due to random point disorder: $\mu = 1/7$, 3/2 or 7/9 depending on the regime [71]. Depinning due to the excitation of half-loops associated with CDs have [73] $\mu = 1$. The traditional Anderson-Kim (AK) regime has [67] $p = -1$. The numerical values of U_p and J_c have limited influence on the values of S. Mathematically, this stems from the fact that S is defined by logarithmic derivatives. These values determine the crossovers among creep regimes in the T-**H** phase diagram.

Several examples of the most common flux creep regimes for YBCO are illustrated in figure 7, where $S(T)$ at 1 T for **H**||c is plotted for seven samples with dissimilar pinning landscapes. We first note that, for a given T, all the samples (with the exception of sample #C, discussed below) have S values within a factor of two of each other, in spite of the fact that their J_c's span a range of almost two orders of magnitude, particularly at high T.

At low T up to ~10 K, all samples have similar creep rates, with $S(T)$ increasing monotonically with T. This is the AK regime in which, as we have shown recently [74], creep for all YBCO samples is close to the universal lower limit given by $S_{AK}(T) \sim Gi^{1/2}(T/T_c)$, where Gi is the Ginzburg number. In

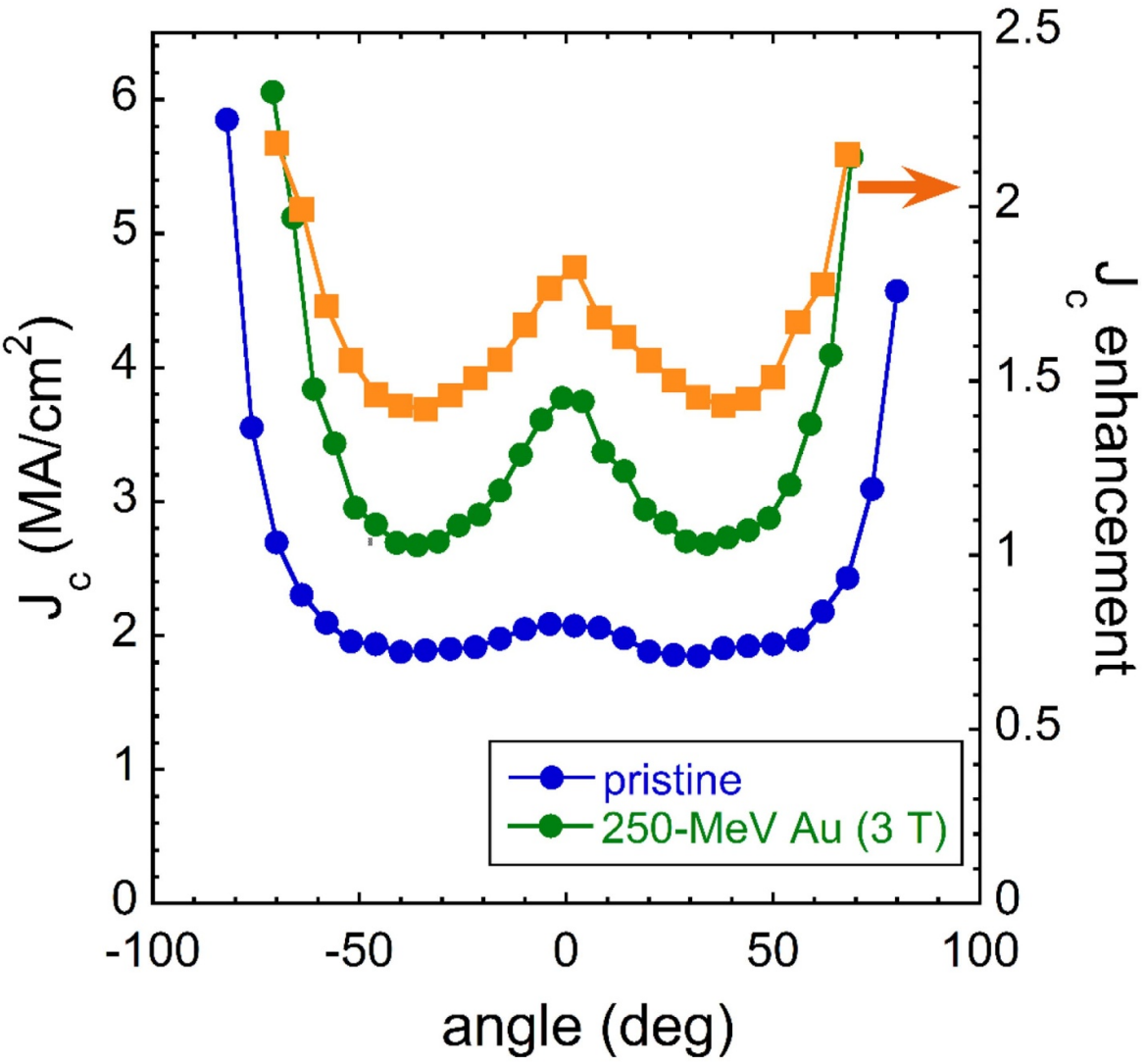

Figure 6. Critical current density (J_c) measured by transport vs. applied magnetic field orientation at $T = 27$ K and $\mu_0 H = 6$ T for a CC from the same batch as the samples shown in figures 2 and 4, before (blue curve) and after (green curve) 250 MeV Au irradiation to $B_\phi = 3$ T along the c-axis (0°). The orange curve shows the enhancement factor.

addition, there is a nonzero $S(T \to 0)$ extrapolation that is frequently attributed to a T-independent quantum creep component S_Q. At high T (above ~60 K), $S(T)$ for all samples increases fast with increasing T, signalling the crossover from glassy to plastic creep [72] and the approach to the irreversibility line.

At intermediate T (between ~10 K and ~60 K), there are basically three types of $S(T)$ curves. Many samples exhibit a large T-independent 'plateau' arising from the glassy 3D collective pinning regime of vortex bundles [75], $S \sim [\mu ln(t/t_0)]^{-1}$, where t_0 is a microscopic attempt time. Examples for this behavior are seen in samples A and E in figure 7, both of which have pinning dominated by random distributions of point defects or small clusters, although the density of such defects is far greater in E than in A. The second category consists of samples with CDs, which develop a maximum in $S(T)$ at intermediate T arising from the expansion of double kinks [64, 65, 68, 73, 76]. In the case of perfectly parallel CDs, initial double-kink expansion should not be glassy [77] (because the kinks have finite sizes) and should turn glassy with a low $\mu \sim 1/3$ (at low H) as J decreases [64, 65, 73, 76, 77]. The result is a very large $S(T)$ peak as in the case of the single crystal C, where CDs with negligible splay were produced by very energetic heavy-ions (1 GeV Au) [65]. A number of strategies can be used to reduce the height of the technologically undesirable $S(T)$ peak by moderating the double-kinks expansion. The first option is to introduce splay among the CDs [64, 65] to geometrically constrain the kinks propagation. An example of this situation is realized in sample B, a single crystal with splayed CDs produced by less energetic ions (0.6 GeV Sn). The double kinks peak is still clearly visible, but it is smaller than in A. The second option is the incorporation of localized defects in between the CDs [15] to pin the kinks. Sample F, a film grown by Pulsed Laser Deposition containing splayed self-assembled $BaZrO_3$ nanorods as well as randomly distributed nanoparticles, is an example of combining both strategies, and consistently the height of the peak is even smaller than in B. The third category of S(T) curves are MOD films with pinning dominated by randomly

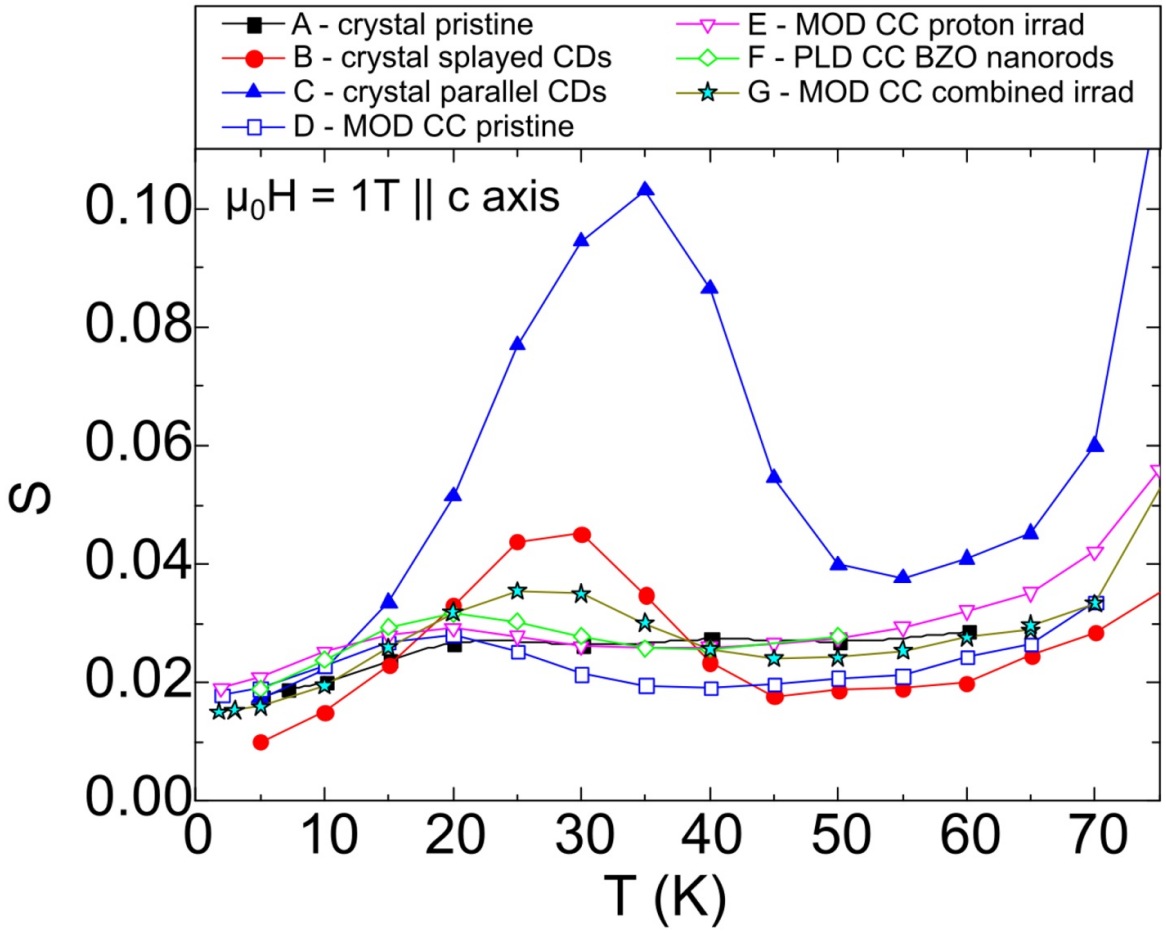

Figure 7. Normalized flux creep rate ($S = d\ln J_c/\ln t$) vs. temperature at an applied magnetic field $\mu_0 H = 1$ T parallel to the c axis, for several YBCO single crystals, thin films and CCs, see text for details. Data for crystal A from Civale *et al* [39], data for B and C form Civale *et al* [65], data for F from Maiorov *et al* [15].

dispersed nanoparticles [17, 51, 72], which exhibit a minimum in $S(T)$ at low H and intermediate T, as our pristine film D (the minimum is more pronounced al lower H, see figure 6 in Eley *et al* [51].). In several previous studies, we have observed that irradiation of the MOD films with light particles that introduce point defects and small clusters increases S at low H and intermediate T, eliminating the minimum and recovering the plateau (sample E) [48–51].

Finally, curve G in figure 7 corresponds to our combined-irradiation CC. These data show the characteristic $S(T)$ peak due to CDs, but the height is smaller than for sample B. Similarly to the case of sample F, this strongly reduced double-kink expansion, which is technologically desirable, is due to the combination of the two factors discussed above, namely, CDs that are splayed and inhomogeneous along their length as well as the presence of p-irradiation induced additional defects to pin the kinks.

Figure 8 shows $S(T)$ curves for the combined irradiation sample at several fields, as well as the $\mu_0 H = 1$ T curve for the pristine film D shown in figure 7 (dashed red curve). The double-kink peak is expected to be highest at the lowest fields, when vortex-vortex interactions can be neglected and each vortex pinned in a CD has plenty of nearby unoccupied CDs where kinks can propagate. This is the condition where the initial non-glassy and later glassy with $\mu = 1/3$ dynamics is expected [64, 65, 73, 76, 77, 78]. It has been shown [64] that splay should increase the glassy exponent to $\mu \sim 0.6$, thus reducing the height of the peak from $S \sim [\mu ln(t/t_0)]^{-1} \sim 0.11$ to ~ 0.05. Unfortunately, there are no theoretical estimates for μ in the presence of localized disorder in between the CDs, nor of how both effects would combine. In any case, we can take the maximum S ~ 0.036 for $\mu_0 H = 0.3$ T to estimate $\mu \sim 0.9$. Vortex-vortex interactions will stiffen the lattice, reducing S. Interactions will increase with increasing T, due to the increase of the transverse vortex localization length and the proliferation of kinks, producing the observed decrease in $S(T)$ with increasing T after it peaks, see figures 7 and 8. Increases in H will also increase the interactions, producing two effects: the $S(T)$ peak will shift to lower T and decrease in height. Both expectations are clearly observed in figure 8; in particular, as shown in the inset, the peak vanishes above $B_\Phi = 4$ T when all CDs are occupied and individual vortex double kink propagation stops (and are replaced by vortex bundle excitations).

Comparison of the $\mu_0 H = 1$ T curves for the pristine and irradiated CCs in figure 7 (curves D and G) and figure 8 shows that they are similar for $T \leq 15$ K. This is fully consistent with the observation that the double irradiation does not

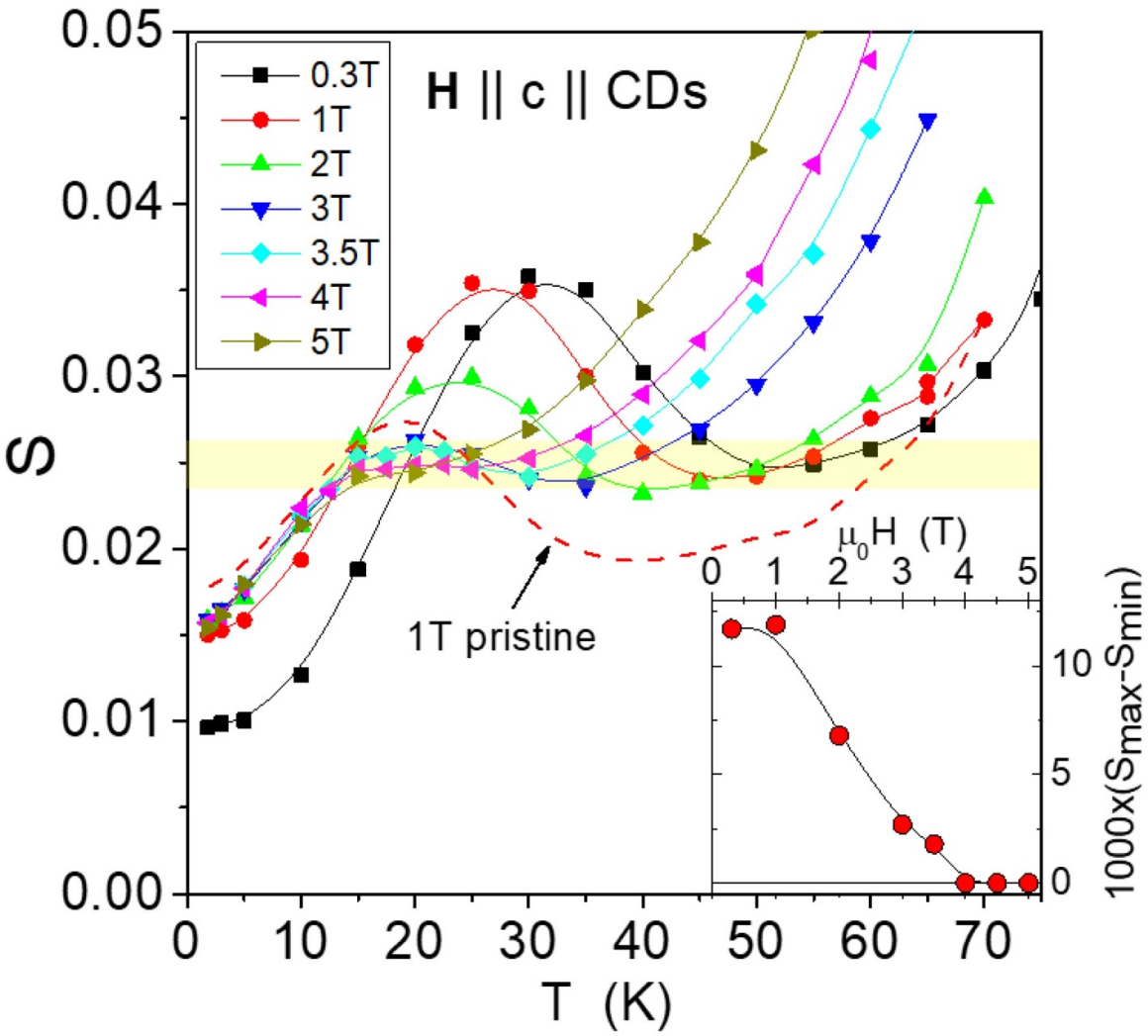

Figure 8. Normalized flux creep rate ($S = d\ln J_c/\ln t$) vs. temperature at several strengths of applied magnetic field (H) parallel to the c axis for the CC piece of this study. The dashed red curve shows the result for a pristine CC (sample D in figure 6) at $\mu_0 H = 1$ T. Inset: Height of the relaxation peak as a function of H.

significantly affect J_c at low T and H, as discussed before. It is also clear that the minimum in $S(T)$ at ∼45 K associated with NPs, well developed in the pristine sample, disappears after irradiation. This is consistent with our previous finding that, for the $S(T)$ minimum to occur, NPs not only have to be present, they must be the *dominant* pinning source [51]. Finally, it is worth noticing that in figure 8, outside the *T*-*H* regions where the dynamics is dominated by double kinks or NPs, all the $S(T, H)$ data converges into a narrow plateau at $S \sim 0.025$ (light yellow band) corresponding to the 'standard' collective creep of bundles ($\mu \sim 1.3$), and suggesting that the dynamics is dominated by point and small-clusters defects.

4. Conclusion

YBCO-based CCs constitute the extreme case of the present capability to create an effective vortex pinning landscape. Successful nanoengineering of the disorder to produce any further J_c enhancement is a hard materials science challenge that requires a deep understanding of the many body system formed by the interacting vortices and the complex defects structure. We have shown that the performance of commercial CCs with artificial pinning centers (chemically incorporated second-phase nanoparticles) can be further improved by combining irradiations with swift Au ions and few MeV protons, which create splayed, non-uniform columnar defects and a combination of point and small-cluster defects, respectively. The resulting J_cs show striking synergies and are higher than those achieved by any of the individual irradiations, in particular in the region of magnetic fields of a few Tesla and intermediate temperatures that is relevant for applications. The effectiveness of this pinning landscape is a consequence of the synergistic pinning effects among the defects of different morphology and hints that even further performance improvements may be possible.

Acknowledgments

Particle irradiation, measurements of vortex creep and magnetization hysteresis and their analysis were supported as part of the Center for Emergent Superconductivity, an Energy Frontier Research Center funded by the U.S. Department of Energy, Office of Science, and Office of Basic Energy Sciences. Angular dependent magnetoresistance measurements were supported by the U. S. Department of Energy, Office of Science, Basic Energy Sciences, Materials Sciences and Engineering Division. Electron microscopy was performed in the Electron Microscopy Center at the Center for Nanoscale Materials, a U.S. Department of Energy Office of Science User Facility under Contract No. DE-AC02-06CH11357. S. E. acknowledges support from the National Science Foundation under Grant No. 1905909 (manuscript preparation).

ORCID iDs

K J Kihlstrom https://orcid.org/0000-0002-9031-1261
G Ghigo https://orcid.org/0000-0003-3368-1319
F Laviano https://orcid.org/0000-0002-5271-6575
M Leroux https://orcid.org/0000-0001-9778-323X

References

[1] Malozemoff A P 2012 *Annu. Rev. Mater. Res.* **42** 373
[2] Shiohara Y, Taneda T and Yoshizumi M 2012 *Jpn. J. Appl. Phys.* **51** 010007 Part 1
[3] Obradors X and Puig T 2014 *Supercond. Sci. Technol.* **27** 044003
[4] Weijers H W *et al* 2014 *IEEE Trans. Appl. Supercond.* **24** 1
[5] Senatore C, Alessandrini M, Lucarelli A, Tediosi R, Uglietti D and Iwasa Y 2014 *Supercond. Sci. Technol.* **27** 103001
[6] Kramer D 2018 *Phys. Today* **71** 25
[7] Foltyn S R, Civale L, MacManus-Driscoll J L, Jia Q X, Maiorov B, Wang H and Maley M 2007 *Nat. Mater.* **6** 631
[8] MacManus-Driscoll J L, Foltyn S R, Jia Q X, Wang H, Serquis A, Civale L, Maiorov B, Hawley M E, Maley M P and Peterson D E 2004 *Nat. Mater.* **3** 439
[9] Haugan T, Barnes P N, Wheeler R, Meisenkothen F and Sumption M 2004 *Nature* **430** 867
[10] Yamada Y *et al* 2005 *Appl. Phys. Lett.* **87** 132502
[11] Kang S *et al* 2006 *Science* **311** 1911
[12] Gutierrez J *et al* 2007 *Nat. Mater.* **6** 367
[13] Holesinger T G *et al* 2008 *Adv. Mater.* **20** 391
[14] Mele P, Matsumoto K, Horide T, Ichinose A, Mukaida M, Yoshida Y, Horii S and Kita R 2008 *Supercond. Sci. Technol.* **21** 032002
[15] Maiorov B, Baily B A, Zhou H, Ugurlu O, Kennison J A, Dowden P C, Holesinger T G, Foltyn S R and Civale L 2009 *Nat. Mater.* **8** 398
[16] Rupich M W *et al* 2010 *Supercond. Sci. Technol.* **23** 014015
[17] Miura M, Maiorov B, Baily S A, Haberkorn N, Willis J O, Marken K, Izumi T, Shiohara Y and Civale L 2011 *Phys. Rev.* B **83** 184519
[18] Miura M, Maiorov B, Willis J O, Marken K, Kato T, Sato M, Shiohara Y and Civale L 2013 *Supercond. Sci. Technol.* **26** 035008
[19] Miura M, Maiorov B, Balakirev F F, Kato T, Sato M, Takagi Y, Izumi T and Civale L 2016 *Sci. Rep.* **6** 20436
[20] Miura M *et al* 2017 *NPG Asia Mater.* **9** e447
[21] Tobita H, Notoh K, Higashikawa K, Inoue M, Kiss T, Kato T, Hirayama T, Yoshizumi M, Izumi T and Shiohara Y 2012 *Supercond. Sci. Technol.* **25** 062002
[22] Xu A, Delgado L, Khatri N, Liu Y, Selvamanickam V, Abraimov D, Jaroszynski J, Kametani F and Larbalestier D C 2014 *APL Mater.* **2** 046111
[23] Xu A *et al* 2017 *Sci. Rep.* **7** 6853
[24] Selvamanickam V, Gharahcheshmeh M H, Xu A, Zhang Y and Galstyan E 2015 *Supercond. Sci. Technol.* **28** 072002
[25] Selvamanickam V, Gharahcheshmeh M H, Xu A, Galstyan E, Delgado L and Cantoni C 2015 *Appl. Phys. Lett.* **106** 032601
[26] Majkic G, Pratap R, Xu A, Galstyan E and Selvamanickam V 2018 *Sci. Rep.* **8** 6982
[27] Lee P J 'Comparisons of superconductor critical current densities' https://nationalmaglab.org/magnet-development/applied-superconductivity-center/plots
[28] Sadovskyy I A *et al* 2016 *Adv. Mater.* **28** 4593
[29] Maiorov B, Katase T, Usov I O, Weigand M, Civale L, Hiramatsu H and Hosono H 2012 *Phys. Rev.* B **86** 094513
[30] Kwok W K, Welp U, Glatz A, Koshelev A E and Kihlstrom K J 2016 *Rep. Prog. Phys.* **79** 116501
[31] Zhu Y, Cai Z X, Budhani R C, Suenaga M and Welch D O 1993 *Phys. Rev.* B **48** 6436
[32] Kirk M A 1993 *Cryogenics* **33** 235
[33] Toulemonde M, Bouffard S and Studer F 1994 *Nucl. Instrum. Methodes Phys. Res.* B **91** 108
[34] Yan Y and Kirk M A 1998 *Phys. Rev.* B **57** 6152
[35] Kirk M A and Yan Y 1999 *Micron* **30** 507
[36] Lang M, Devanathan R, Toulemonde M and Trautmann C 2015 *Curr. Opin. Solid State Mater. Sci.* **19** 39
[37] Sadovskyy I A, Koshelev A E, Glatz A, Ortalan V, Rupich M V and Leroux M 2016 *Phys. Rev. Appl.* **5** 014011
[38] Ghigo G, Laviano F, Gerbaldo R and Gozzelino L 2012 *Supercond. Sci. Technol.* **25** 115007
[39] Civale L, Marwick A D, McElfresh M W, Worthington T K, Malozemoff A P, Holtzberg F H, Thompson J R and Kirk M A 1990 *Phys. Rev. Lett.* **65** 1164
[40] van Dover R B, Gyorgy E M, White A E, Schneemeyer L F, Felder R J and Waszczak J V 1990 *Appl. Phys. Lett.* **56** 2681
[41] Giapintzakis J, Lee W C, Rice J P, Ginsberg D M, Robertson I M, Wheeler R, Kirk M A and Ruault M O 1992 *Phys. Rev.* B **45** l0677
[42] Umezawa A, Crabtree G W, Liu J Z, Weber H W, Kwok H K, Nunez L H, Moran T J, Sowers C H and Claus H 1987 *Phys. Rev.* B **36** 7151
[43] Sauerzopf F M, Wiesinger H P, Kritscha W, Weber H W, Crabtree G W and Liu J Z 1991 *Phys. Rev.* B **43** 3091
[44] Weber H W 1992 *Progress in High Temperature Superconductivity* vol 31 (Singapore: World Scientific)
[45] Civale L, Marwick A D, Worthington T K, Kirk M A, Thompson J R, Krusin-Elbaum L, Sun Y, Clem J R and Holtzberg F 1991 *Phys. Rev. Lett.* **67** 648
[46] Konczykowski M, Rullier-Albenque F, Yacoby E R, Shaulov A, Yeshurun Y and Lejay P 1991 *Phys. Rev.* B **44** 7167
[47] Laviano F, Xie R, Mezzetti E and Kwok W K 2008 *Phys. Rev.* B **77** 214501
[48] Jia Y *et al* 2013 *Appl. Phys. Lett.* **103** 122601
[49] Leroux M *et al* 2015 *Appl. Phys. Lett.* **107** 192601
[50] Rupich M W *et al* 2016 *IEEE Trans. Appl. Supercond.* **26** 6601904
[51] Eley S, Leroux M, Rupich M W, Miller D J, Sheng H, Niraula P M, Kayani A, Welp U, Kwok W K and Civale L 2017 *Supercond. Sci. Technol.* **30** 015010
[52] Leonard K J, Aytug T, List F A, Perez-Bergquist A, Weber W J and Gapud A 2013 Fusion Reactor Materials Program, June 30, DOE/ER-0313/54 vol 54 p 125

[53] Leonard K J, Aytug T, List F A, Perez-Bergquist A, Weber W J and Gapud A 2013 Fusion Reactor Materials Program, December 31, DOE/ER-0313/55 vol 55 p 54
[54] Leonard K J, Aytug T, Gapud A, List F A, Greenwood N T, Zhang Y W, Perez-Bergquist A and Weber W J 2014 *Fusion Sci. Technol.* **66** 57
[55] Hua J, Welp U, Schlueter J, Kayani A, Xiao Z L, Crabtree G W and Kwok W K 2010 *Phys. Rev.* B **82** 024505
[56] Kihlstrom K J *et al* 2013 *Appl. Phys. Lett.* **103** 202601
[57] Rupich M W, Verebelyi D T, Zhang W, Kodenkandath T and Li X 2004 *MRS Bull.* **29** 572
[58] Li X *et al* 2009 *IEEE Trans. Appl. Supercond.* **19** 3231
[59] Rupich M W, Li X, Sathyamurthy S, Thieme C, DeMoranville K, Gannon J and Fleshler S 2013 *IEEE Trans. Appl. Supercond.* **23** 6601205
[60] Bean C P 1964 *Rev. Mod. Phys.* **36** 31
[61] Koshelev A E, Sadovskyy I A, Phillips C L and Glatz A 2016 *Phys. Rev.* B **93** 060508
[62] Willa R, Koshelev A E, Sadovskyy I A and Glatz A 2018 *Supercond. Sci. Technol.* **31** 014001
[63] Leroux M *et al* 2019 *PNAS* **116** 10691
[64] Hwa T, Le Doussal P, Nelson D R and Vinokur V M 1993 *Phys. Rev. Lett.* **71** 3545
[65] Civale L, Krusin-Elbaum L, Thompson J R, Wheeler R, Marwick A D, Kirk M A, Sun Y R, Holtzberg F and Feild C 1994 *Phys. Rev.* B **50** 4102
[66] Civale L 1997 *Supercond. Sci. Technol.* **10** 184519
[67] Anderson P W and Kim Y B 1964 *Rev. Mod. Phys.* **36** 39
[68] Blatter G, Feigel'man M V, Geshkenbein V B, Larkin A I and Vinokur V M 1994 *Rev. Mod. Phys.* **66** 1125
[69] Yeshurun Y, Malozemoff A P and Shaulov A 1996 *Rev. Mod. Phys.* **68** 911
[70] Fisher M P A 1989 *Phys. Rev. Lett.* **62** 1415
[71] Feigel'man M V, Geshkenbein V B, Larkin A I and Vinokur V M 1989 *Phys. Rev. Lett.* **63** 2303
[72] Haberkorn N *et al* 2012 *Phys. Rev.* B **85** 174504
[73] Nelson D R and Vinokur V M 1992 *Phys. Rev. Lett.* **68** 2398
[74] Eley S, Miura M, Maiorov B and Civale L 2017 *Nat. Mater.* **16** 409
[75] Malozemoff A P and Fisher M P A 1990 *Phys. Rev.* B **42** 6784
[76] Thompson J R, Krusin-Elbaum L, Civale L, Blatter G and Feild C 1997 *Phys. Rev. Lett.* **78** 3181
[77] Niebieskikwiat D, Civale L, Balseiro C A and Nieva G 2000 *Phys. Rev.* B **61** 7135
[78] Krusin-Elbaum L, Civale L, Thompson J R and Feild C 1996 *Phys. Rev.* B **53** 11744